Available online at www.sciencedirect.com
ScienceDirect
Geochimica et Cosmochimica Acta 73 (2009) 7110–7126
Geochimica et Cosmochimica Acta
www.elsevier.com/locate/gca

Experimental calibration of oxygen isotope fractionation between quartz and zircon

Dustin Trail [a,*], Ilya N. Bindeman [b], E. Bruce Watson [a], Axel K. Schmitt [c]

[a] Department of Earth & Environmental Sciences, Rensselaer Polytechnic Institute, Troy, NY 12180, USA
[b] Department of Geological Sciences, University of Oregon, Eugene, OR 97403, USA
[c] Department of Earth and Space Sciences & Institute of Geophysics and Planetary Physics, University of California, Los Angeles, CA 90095, USA

Received 6 January 2009; accepted in revised form 20 August 2009; available online 26 August 2009

Abstract

We report the results of an experimental calibration of oxygen isotope fractionation between quartz and zircon. Data were collected from 700 to 1000 °C, 10–20 kbar, and in some experiments the oxygen fugacity was buffered at the fayalite–magnetite–quartz equilibrium. Oxygen isotope fractionation shows no clear dependence on oxygen fugacity or pressure. Unexpectedly, some high-temperature data (900–1000 °C) show evidence for disequilibrium oxygen isotope partitioning. This is based in part on ion microprobe data from these samples that indicate some high-temperature quartz grains may be isotopically zoned. Excluding data that probably represent non-equilibrium conditions, our preferred calibration for oxygen isotope fractionation between quartz and zircon can be described by:

$$1000 \ln \alpha_{qtz\text{–}zrc} = (2.33 \pm 0.24) \times 10^6/T^2(\text{in K})$$

This relationship can be used to calculate fractionation factors between zircon and other minerals. In addition, results have been used to calculate WR/melt–zircon fractionations during magma differentiation. Modeling demonstrates that silicic magmas show relatively small changes in $\delta^{18}O$ values during differentiation, though late-stage mafic residuals capable of zircon saturation contain elevated $\delta^{18}O$ values. However, residuals also have larger predicted melt–zircon fractionations meaning zircons will not record enriched $\delta^{18}O$ values generally attributed to a granitic protolith. These results agree with data from natural samples if the zircon fractionation factor presented here or from natural studies is applied.

1. INTRODUCTION

Zircon is a common accessory phase found in many crustal rocks and is often present with quartz. Oxygen isotope compositions of quartz in rocks have helped characterize petrogenetic processes for about half a century (Taylor, 1968; Taylor and Sheppard, 1986). More recently, an increasing number of zircon oxygen isotope data have been used to gain new insight into crustal evolution (e.g., Valley et al., 1994, 2005; Bindeman et al., 2008). In addition, since zircon is resistant to physical and chemical breakdown during weathering, oxygen isotope ratios of detrital grains have also been used to constrain source melt compositions (e.g., Valley et al., 2005; Cavosie et al., 2005; Trail et al., 2007). The application of $\delta^{18}O$ values in zircon to petrological problems depends upon the characterization of an equilibrium fractionation behavior. For example, equilibrium fractionation between quartz and zircon at $\geqslant 500$ °C is predicted by the following equation:

$$\delta^{18}O(qtz) - \delta^{18}O(zrc) \approx 10^3 \ln \alpha_{qtz\text{–}zrc} = \frac{A_{qtz\text{–}zrc} \times 10^6}{T^2\ (\text{in K})} \quad (1)$$

where $\alpha_{qtz\text{–}zrc}$ is the fractionation factor—the $^{18}O/^{16}O$ ratio in quartz divided by the $^{18}O/^{16}O$ ratio in zircon—and linearity is assumed for $1000 \ln \alpha$ vs. $1/T^2$ (Bottinga and Javoy, 1973).

* Corresponding author. Fax: +1 518 276 2012.
E-mail address: traild@rpi.edu (D. Trail).

0016-7037/$ - see front matter © 2009 Elsevier Ltd. All rights reserved.
doi:10.1016/j.gca.2009.08.024

Thus, $A_{qtz-zrc}$ can be solved knowing temperature and the oxygen isotope composition of quartz and zircon, although polynomial functions are sometimes used for experimental and theoretical calibrations (Clayton and Kieffer, 1991).

The purpose of this contribution is to present the results of new experiments that constrain the temperature dependence of oxygen isotope fractionation between quartz and zircon. Unlike other igneous minerals such as feldspars that may have isotope fractionations that depend on cation chemistry because they are solid solutions, quartz and zircon contain relatively minor cation impurities that do not influence oxygen isotope fractionations. Because of the ubiquity of quartz and zircon in crustal rocks, the importance of zircon as a geochemical tool, the widespread use as a crustal geochronometer, and the abundance of oxygen isotope data collected from both minerals, a robust calibration would have wide application. The potential exists, for example, to compare quartz–zircon isotopic temperatures to temperatures derived from Ti-in-zircon and zircon saturation thermometry (Watson and Harrison, 1983, 2005; Ferry and Watson, 2007), and to further characterize oxygen isotope equilibrium (or disequilibrium). In addition, the provenance of detrital zircons is a common target of study whose significance is heightened by the recognized existence of crystals older than the known rock record (e.g. Harrison et al., 2005). Provided zircon crystallization temperatures can be estimated (Watson et al., 2006; Ferry and Watson 2007), host rock characteristics could be further constrained. Finally, since quartz–mineral fractionation factors have been measured for many other phases, calculation of mineral–zircon and melt–zircon fractionation factors are possible with reasonable assumptions.

2. METHODS

2.1. Experimental design and setup

Our experimental design was based on a few notable observations from previous oxygen isotope experimental studies. First, dry direct-exchange experiments (i.e., with calcite) were not considered because zircon does not readily recrystallize, and oxygen diffusion in zircon is slow (Watson and Cherniak, 1997) making laboratory experiments time-prohibitive. In addition, this is probably an ineffective means to determine a zircon fractionation factor, since experiments demonstrated that, in the absence of quartz, zircon reacts with calcite to form baddeleyite (Sessions et al., 1996). The application of the three-isotope method to determine equilibrium fractionation between two minerals directly (Shahar et al., 2008) was ruled out because it relies on the expectation that phases do not substantially dissolve and re-precipitate in the presence of a solvent (Matsuhisa et al., 1978; Shahar et al., 2008). In other words, this approach is probably unsuitable here because SiO_2 is soluble in H_2O at run conditions, and the solubility varies substantially with temperature and pressure (Manning, 1994). Finally, zircon–fluid fractionation experiments were not considered because the dissolved species of the aqueous fluid depends on the mineral, and can change with temperature, meaning it may be problematic to combine two mineral-H_2O experimental data sets to achieve accurate fractionation factors. This effect was termed the "salt effect" and is described in Hu and Clayton (2003).

Therefore, we synthesized quartz and zircon in the presence of aqueous fluid in a piston-cylinder apparatus at temperatures ranging from 700 to 1000 °C, and pressures of 10 and 20 kbar in Ag or Pt capsules. While this method is rarely used to characterize equilibrium fractionation factors for minerals, it has proved successful in the past. For example, Downs et al. (1981) synthesized quartz and magnetite from 600 to 800 °C; an $A_{qtz-mag}$ value of 6.31 can be calculated from this data set. This is in good agreement with later $A_{qtz-mag}$ values of 6.11 and 6.29 determined by different techniques (Matthews et al., 1983a; Chiba et al., 1989).

Our starting materials were synthetic baddeleyite ($\leqslant$1 μm), amorphous SiO_2, and distilled water. Molar ratios were chosen such that water and dissolved SiO_2 (i.e., the fluid) comprised ~80% of the total oxygen, as determined by SiO_2 solubility in H_2O (Manning, 1994). The additional 20% was made up of the same number of oxygen atoms of zircon and quartz synthesis material (10% each). These proportions were chosen to maximize the fluid molar content, while still providing enough material for isotope analyses. Initial experiments revealed that the abundance of zircon inclusions in quartz were high enough to affect isotope measurements. We modified the experimental setup so that both phases would crystallize in chemical communication but would be easily separable for isotope analysis. This was accomplished with a nested capsule, and chemical communication was obtained through circulation of hydrothermal fluid (Watson et al., 2006). In some experiments, the oxygen fugacity (fO_2) was buffered at the fayalite–magnetite–quartz buffer (FMQ). Sketches of experimental designs can be found in Fig. 1.

Throughout the course of our exploratory experiments, incomplete reaction of baddeleyite + SiO_2 to zircon was observed; in some cases, up to 20% of the baddeleyite remained, and was armored by zircon. Assuming that baddeleyite and zircon have $\delta^{18}O$ values that differ by no more than ~2‰ at 700 °C equilibrium, and that baddeleyite exchanged and equilibrated with the aqueous fluid—reasonable given final grain size, diffusivities of O in zircon, and run duration—an uncertainty of ~0.4‰ would be propagated into the accuracy of zircon measurements. While the above calculation assumes diffusive equilibrium based on the diffusivities of O in zircon (Watson and Cherniak, 1997), the full reaction of baddeleyite to zircon is rate limited by Si diffusion in zircon, which is 10 orders of magnitude slower than O diffusion at 700 °C (Watson and Cherniak, 1997; Cherniak, 2008).

A few modifications to the experimental setup were found to significantly decrease the contaminant content. We adjusted the inner capsule SiO_2:ZrO_2 ratio such that SiO_2 was in ~10% greater abundance than in stoichiometric zircon, and increased heating rates from 100 °C/min up to 300°/min. In addition, experiment duration was increased, especially for experiments at lower temperatures, and time series experiments were performed. Under this experimental protocol, approximately 30% of the runs contained adequate material for isotope analysis, though no runs at

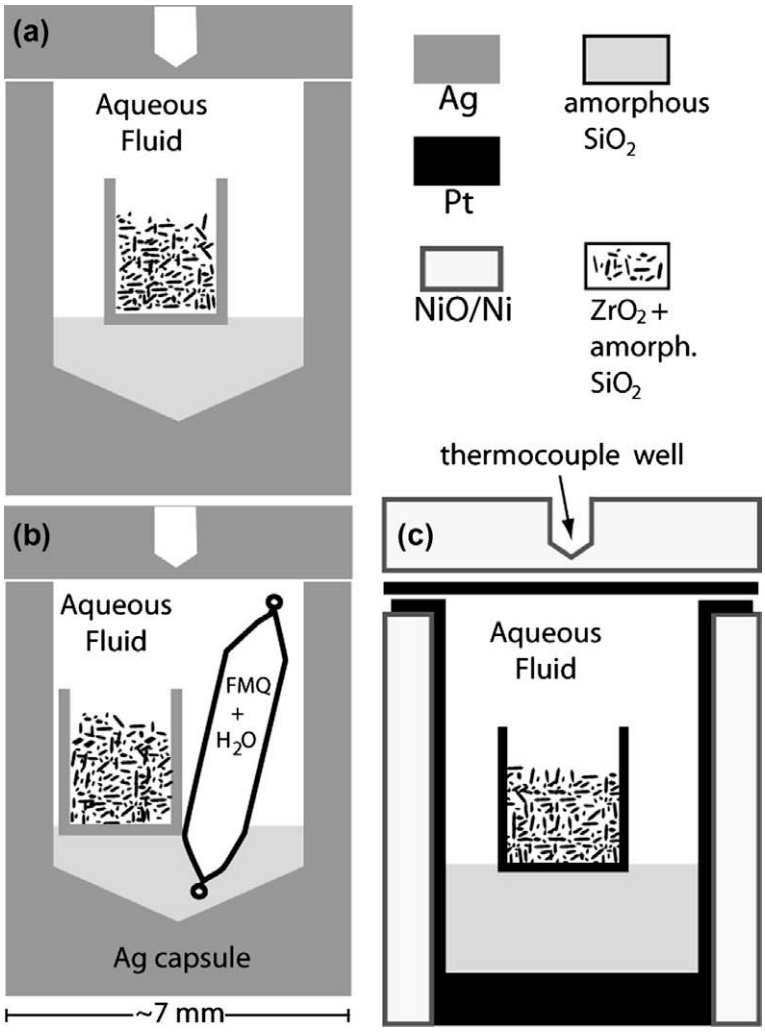

Fig. 1. Sketches of experimental designs used in this study. All experiments contained an inner capsule where zircon source material was placed, which prevented zircon inclusions in quartz grains. Aqueous fluid provided chemical communication between the two phases; the thermocouple well was packed with MgO. The standard piston-cylinder assembly (not shown) is similar to that described in Watson et al. (2006). (a) The conventional setup used for most of our experiments contained inner and outer Ag capsules. These capsules were stored in ethanol alcohol which kept Ag oxide from forming on the surface. Capsules were free of Ag oxide at run completion; this is expected because inspection of Ellingham diagram shows that Ag oxide is not stable at temperatures greater than 200 °C. (b) In some experiments, the oxygen fugacity was buffered at FMQ. This was accomplished by including a welded Pt capsule with FeO + silicic acid, which reacted to form fayalite, magnetite, and quartz + H_2O. Since Pt is permeable to H_2, the fH_2 in the capsule and buffer become equal, thus buffering the fO_2. (c) For 1000 °C runs, an oxidized Ni holder was lined with a Pt capsule and gasket, which ensured a watertight seal during pressurization. The inner capsule was also Pt.

temperatures less than 700 °C produced sufficient reaction to include in our final calibration. We assessed baddeleyite contamination in zircon with image analysis software of backscattered electron (BSE) images of zircon in every run product. On average, baddeleyite contaminant was reduced to ~3%, and using similar assumptions described above, this would propagate an error of ~0.1‰ into the final measured zircon value. While the $\delta^{18}O$ values of ZrO_2 (+13.3‰) and SiO_2 (+11.3‰) source material were held constant throughout the course of our experiments, three separate H_2O compositions (−5 to +15‰) were used, though with no apparent affect on the final $\Delta^{18}O$(qtz–zrc) value was observed.

All capsules were moist upon opening. Quartz grains were separated from the run products, cleaned in ethanol, sonicated, and inspected for inclusions by reflected light, transmitted light, and backscattered electron imaging. Zircon grains produced in our run products were too small for hand picking, (~5 μm) so grains were treated in cold HF acid overnight to remove any residual SiO_2 quench material or small quartz grains.

2.2. Laser fluorination

Oxygen isotope compositions of quartz and zircon were measured by laser fluorination at the University of Oregon

Stable Isotope Lab using a 35 W CO_2-laser. The individual mineral separates weighed 0.6–1 mg, and measurements were duplicated when experimental material allowed. Samples were reacted with BrF_5, and unknowns were monitored against University of Wisconsin garnet standard UWG-2 (Valley et al., 1995) and internal lab standard Bishop Tuff quartz (sample LV748; Bindeman and Valley, 2002). Oxygen was converted to CO_2 gas, and analyzed on a MAT 253 mass spectrometer integrated with the laser line. Quartz grains were measured using the rapid heating defocused beam technique which was demonstrated to produce $\delta^{18}O$ values independent of grain size (Spicuzza et al., 1998). Quartz grains showed no crystal jumping, which suggests they were largely free of fluid inclusions, and yields were ~100%, similar to Bishop Tuff quartz. Yields for zircons ranged from 55% to 75% depending on the amount of granular zircon loss upon initial laser pulse scattering. Partial yields for multiple zircons analyzed by laser fluorination is observed in stable isotope labs (e.g., Valley et al., 2005) and do not affect $\delta^{18}O$ values (e.g. Wiedenbeck et al., 2004), likely because the temperature of zircon BrF_5 reaction exceeds 2000 °C; at such temperatures it is assumed that isotope fractionations between reaction products are virtually zero. It is also worth noting that zircon from these experiments lased more smoothly and produced higher yields than laser fluorination measurements routinely made on natural zircons.

In addition, nine aliquots of Bishop Tuff quartz were measured in two analytical sessions and yielded $\delta^{18}O$ values of $8.20 \pm 0.08‰$ (1σ) and $8.27 \pm 0.13‰$ (1σ) calibrated relative to the UWG-2 garnet standard (EA-1). These values are identical within error to the previously reported value from the University of Wisconsin laser fluorination lab ($+8.24 \pm 0.08‰$ (1σ); Bindeman and Valley, 2002). Since zircon values presented here are also calibrated relative to the UWG-2 standard, this provides strong evidence against any measurement-related $\Delta^{18}O$(qtz–zrc) fractionations of these two minerals or inter-laboratory differences.

2.3. Ion microprobe

Unexpectedly, the highest temperature runs exhibited large variations in $\Delta^{18}O$(qtz–zrc) values, and the ion microprobe was used to determine whether quartz grains display measurable heterogeneities by performing spot traverses from the grain centers to the rims. All $\delta^{18}O$ quartz determinations were made using the UCLA CAMECA ims 1270 high-resolution ion microprobe in Faraday multicollection mode. A 2.8–3.1 nA Cs^+ beam was focused to a ~20 μm spot and 10 keV secondary ions were admitted to the mass spectrometer after passing through a 30 eV energy slit, which achieved $\sim 2 \times 10^9$ and $\sim 4 \times 10^6$ counts per second for $^{16}O^-$ and $^{18}O^-$ ions, respectively. A mass resolving power of 2400 was used to resolve hydride interferences, and a liquid nitrogen cold finger helped remove trace condensable gases from the sample chamber. Analysis spots were pre-sputtered for 2 min while background counts were simultaneously monitored on the detectors with the secondary beam deflected.

In order to avoid bias caused by fractionation effects due to mount geometry, all grains were mounted within the inner 1 cm of the epoxy mount, and were carefully polished to ensure that grains were free of relief. Unknowns were arranged so that they geometrically bracketed standards; additionally, standards were analyzed so that they temporally bracketed unknowns (EA-2). Quartz standard UWQ-1 ($\delta^{18}O = +12.33‰$; Kelly et al., 2007) was used along with Bishop Tuff quartz crystals from the same sample discussed in Section 3.2, to further monitor fractionation effects. Errors based on counting statistics are 0.1‰ or less for standards and unknowns. A small drift correction was applied to the data to offset a measured increase of 0.4‰ to UWQ-1 over the 8 h. analytical session, and the standard reproducibility was 0.32‰ (1σ; $n = 38$), representing an estimate for the analytical uncertainty of the ion microprobe quartz measurements. The average corrected $\delta^{18}O$ value of Bishop Tuff quartz analyses, corrected to +12.33‰ UWQ-1 quartz value, is $+8.56 \pm 0.37‰$ (1σ; $n = 10$) which overlaps within uncertainty with laser fluorination values.

3. RESULTS

3.1. Run products

Sample images of zircon and quartz grains can be found in Fig 2. Some zircon grains contain small impurities of ZrO_2, and what are interpreted to be fluid inclusions. It is assumed that fluid inclusions were not a significant source of contamination because of their low frequency of occurrence in BSE images. Zircons increased in size with temperature, from ~3 μm at 700 °C, up to ~5 μm at 1000 °C. Quartz grains also increased in size with temperature, from ~200 μm at 700 °C, to as large as 2 mm for 1000 °C runs. However, a 900 °C run at 20 kbar yielded the smallest quartz grains of all runs (~50 μm); the higher pressure appears to have suppressed quartz grain growth, though it did not affect zircon grain size.

3.2. Oxygen isotope data

All oxygen isotope results are reported according to the conventional $\delta^{18}O$ notation, relative to Vienna Standard Mean Ocean Water (VSMOW), and errors in all cases are reported at one standard deviation. Differences in $^{18}O/^{16}O$ between phases are represented by Δ; for example, $\delta^{18}O_{VSMOW}(qtz) - \delta^{18}O_{VSMOW}(zrc) = \Delta_{qtz-zrc}$. Table 1 presents laser fluorination results from separated zircon and quartz run products, which were (on average) reproducible to ±0.06 and 0.14‰, respectively, compared to the ±0.1‰ reproducibility of UWG-2 standard. Final $\Delta_{qtz-zrc}$ errors are calculated by differencing ($\sqrt{[(err_{qtz})^2 + (err_{zrc})^2]}$), using 1σ errors for quartz and zircon.

The primary goal of the ion microprobe work (Table 2) was to identify intra-grain variations and check for heterogeneities in quartz run products vs. temperature. Results were collected from a suite of quartz grains; some came from aliquots not analyzed by laser fluorination. This was done because residual material remaining from laser fluorination aliquots contained the smallest grains, which could bias results. The last column of Table 2 indicates the

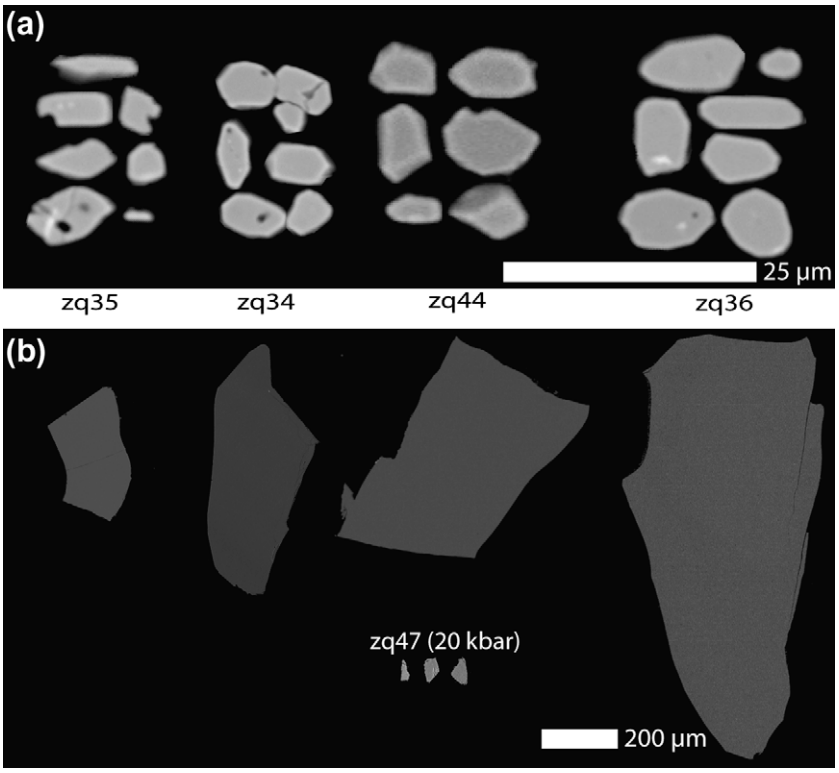

Fig. 2. Backscattered electron images of grains from various run products. (a) Zircon grains from 700 to 1000 °C, from left to right, in increments of 100 °C. Grains contain small inclusions of ZrO_2, (for example see the bottom left grains from zq36). In addition, dark holes which contain no material were believed to be fluid inclusions before grain sectioning (for example, see the bottom left grains of zq35, zq34, and zq36). (b) Quartz grains generally increase in size with increasing temperature and run duration; some notable exceptions are grains that crystallized at higher pressure (zq47; 900 °C, 20 kbar), and grains that crystallized in a capsule with slightly less available "free" space; specifically, in experiments which contained an internal buffer (i.e., zq53, zq66; see Fig. 1b).

location of the ion microprobe traverse (i.e., C = core, I = intermediate, R = rim), and images of quartz grains with ion microprobe spot locations can be found in EA-3.

For all fractionations, $\Delta_{qtz-zrc}$ values are reported using only the laser fluorination data, for two reasons. First, the laser fluorination technique produces data with better precision (approximately ±0.1‰) when compared to the ion microprobe data (approximately ±0.3‰); ion microprobe data will lead to larger errors in the final A value, since the uncertainty in the A value scales as a power law with the standard deviation for the data. In addition, it is possible to introduce small, but systematic shifts into the final $\Delta_{qtz-zrc}$ value by combining two measurement techniques. The results are further discussed below, and grouped according to run temperature; the data are presented in this fashion because some data at certain temperatures are unlikely to be reliable because of erratic $\Delta_{qtz-zrc}$ values.

3.2.1. 700 °C

Laser fluorination data from two 700 °C and 10 kbar runs produced $\Delta_{qtz-zrc}$ values identical to each other within the error of analyses, with run durations of 151 and 431 h. Ion microprobe data for two grains from the 151 h. run (zq35) and another 700 °C run (zq58) demonstrate quartz homogeneity similar to the ion microprobe quartz standards; intra-grain reproducibility of 0.18 and 0.38‰ were calculated by taking the standard deviation of measurements for each individual grain.

3.2.2. 800–875 °C

Three 800 °C experiments at 10 kbar produced laser fluorination $\Delta_{qtz-zrc}$ values from 1.55 to 2.91, and do not show systematic dependence on time (the highest and lowest fractionations occur after similar run times). The highest $\Delta_{qtz-zrc}$ value was from a run with the fO_2 buffered at FMQ. We can see no *a priori* reason why quartz–zircon fractionation would depend on fO_2, but we explored this possibility by conducting another FMQ-buffered experiment at 875 °C. With considerations for the 75 °C temperature increase, the laser fluorination results suggest that the fO_2 does not have a major effect on oxygen isotope fractionation. Quartz grains from four separate 800 °C run products were analyzed by ion microprobe, and the intra-grain standard deviations were $\leqslant 0.34$‰, which is less than or equal to standard reproducibility. Similarly, quartz grains from experiments at 850 and 875 °C (fO_2 buffered) produced an intra-grain standard deviation less than the standard reproducibility.

3.2.3. 900 °C

Two experiments—zq43 and zq47—were performed for similar durations, at pressures of 10 and 20 kbar, and

Table 1
Laser fluorination oxygen isotope data from run products.

Name	Initial H_2O	Phase	T (°C)	P (kbar)	t (h)	$\delta^{18}O_{VSMOW}$ (‰)		(1σ)	n	$\Delta^{18}O$	$10^3 \ln \alpha_{qtz-zrc}$		(1σ)
Start mat'l		ZrO_2				13.3							
Start mat'l		SiO_2(amorph.)				11.3							
zq35	15	Quartz	700	10	151	16.21	±	0.14	3				
zq35	15	Zircon	700	10	151	13.94	±	0.07	2	2.27	2.23	±	0.15
zq49	−5	Quartz	700	10	431	−4.17	±	0.12	3				
zq49	−5	Zircon	700	10	431	−6.66	±	0.07	2	2.49	2.50	±	0.14
zq34	15	Quartz	800	10	89	15.13	±	0.01	2				
zq34	15	Zircon	800	10	89	13.02	±	0.06[a]	1	2.11	2.08	±	0.06
zq51	−5	Quartz	800	10	144	−4.28	±	0.14	3				
zq51	−5	Zircon	800	10	144	−5.83	±	0.10	2	1.55	1.55	±	0.17
zq53[b]	−5	Quartz	800	10	146	−3.02	±	0.20	3				
zq53[b]	−5	Zircon	800	10	146	−5.94	±	0.08	2	2.91	2.93	±	0.21
zq66[b]	−5	Quartz	875	10	146	−3.08	±	0.14[a]	1				
zq66[b]	−5	Zircon	875	10	146	−4.39	±	0.05	4	1.31	1.32	±	0.15
zq43	−3	Quartz	900	10	95	−4.24	±	0.37	2				
zq43	−3	Zircon	900	10	95	−4.63	±	0.00	2	0.40	0.40	±	0.37
zq47	−3	Quartz	900	20	93	−2.81	±	0.14[a]	1				
zq47	−3	Zircon	900	20	93	−4.27	±	0.08	2	1.46	1.47	±	0.16
zq64	−5	Quartz	950	10	72	−2.79	±	0.12	2				
zq64	−5	Zircon	950	10	72	−3.89	±	0.01	2	1.10	1.10	±	0.12
zq52	−5	Quartz	950	10	140	−4.15	±	0.15	3				
zq52	−5	Zircon	950	10	140	−4.91	±	0.06[a]	1	0.76	0.77	±	0.16
zq61	−5	Quartz	950	10	198	−1.17	±	0.03	2				
zq61	−5	Zircon	950	10	198	−0.90	±	0.07	2	−0.27	−0.27	±	0.08
zq36	15	Quartz	1000	10	47	16.42	±	0.12	2				
zq36	15	Zircon	1000	10	47	13.85	±	0.03	2	2.57	2.53	±	0.13
zq44	−3	Quartz	1000	10	93	2.14	±	0.14[a]	1				
zq44	−3	Zircon	1000	10	93	−2.24	±	0.08	2	4.38	4.38	±	0.16

[a] Errors estimated according to average reproducibility of other data.
[b] fO_2 buffered at FMQ.

measured laser fluorination $\Delta_{qtz-zrc}$ fractionations were 0.40 and 1.46, respectively. One ion microprobe spot was collected from a grain from zq47 (20 kbar run), which shows good agreement with the laser fluorination data. Additionally, ion microprobe data were collected from two grains from a separate 10 kbar run (zq65). Because insufficient material remained from zq43, grains from zq65 (900 °C) were chosen as a proxy for zq43. The intra-grain reproducibility was 0.34 and 0.54‰, greater than the analytical variability on standards in one case. Furthermore, laser fluorination analyses on separate quartz grain aliquots from run zq43 yielded a standard deviation of 0.37‰, which is significantly worse than the reproducibility of the standards and of other quartz runs analyzed.

3.2.4. 950 and 1000 °C

Three runs (zq64, zq52, zq61) were performed at 950 °C, for durations of 72, 140, and 198 h, and yielded with laser fluorination $\Delta_{qtz-zrc}$ values of 1.10, 0.76, and -0.27 respectively. Run zq61 was the only measured experiment with a negative $\Delta_{qtz-zrc}$ value. The 1000 °C runs produced two of the three largest fractionations between quartz and zircon from our run products (including the largest), but should have produced the smallest fractionations if the assumptions implicit in the use of Eq. (1) are valid. In addition, the difference between the 1000 °C $\Delta_{qtz-zrc}$ values is the largest for any two measured fractionations collected at the same temperature. Ion microprobe data from zq64 (950 °C) were obtained on two grains, and intra-grain calculated standard deviations were 0.00 and 0.63‰. Additionally, results for two grains from two separate 1000 °C experiments were reproducible to 0.42 and 0.55‰, which are larger than the uncertainty of the standards.

4. THE FRACTIONATION FACTOR FOR ZIRCON

4.1. Kinetic effects

After ruling out analytical problems as a cause of inter-experiment variation in $A_{qtz-zrc}$ values (Section 2.2. and EA-1, EA-2), we hypothesized that kinetic processes may have caused some of the disagreement among values at higher temperatures. A plot of $\Delta_{qtz-zrc}$ vs. time for all run products and intra-grain ion microprobe standard deviations vs. run temperature are summarized in Fig. 3. As shown (Fig 3a), 700–900 °C experiments display no apparent correlation with run duration. However, 950 °C data appear to trend from positive to negative $\Delta_{qtz-zrc}$ values with time. Results from 1000 °C runs are spurious; implied fractionations are not geologically plausible. Additionally, quartz intra-grain heterogeneities may have increased slightly at higher temperatures (Fig. 3b). Grains with the largest standard deviations were collected from runs performed at 900 °C or greater, though it is important to note

Table 2
Ion microprobe data for quartz grains from experimental run products.

Grain@spot	T (°C)	^{16}O (cps)	^{18}O (cps)	$^{18}O/^{16}O$ measured	$^{18}O/^{16}O$ corrected[a]	$^{18}O/^{16}O$ 1σ (internal)	$\delta^{18}O_{VSMOW}$ 1σ (external) (‰)		Spot location[b]
zq35_1@1	700	1.88E + 09	3.81E + 06	0.00202871	0.00203881	1.883E − 07	16.76	0.09	C
zq35_1@2	700	1.92E + 09	3.89E + 06	0.00202820	0.00203829	2.229E − 07	16.50	0.11	R
							16.63	0.18	
zq35_2@1	700	1.77E + 09	3.60E + 06	0.00202921	0.00203965	1.671E − 07	17.18	0.08	R
zq35_2@2	700	1.82E + 09	3.69E + 06	0.00202777	0.00203819	2.093E − 07	16.45	0.10	I
zq35_2@3	700	1.79E + 09	3.63E + 06	0.00202890	0.00203931	2.477E − 07	17.01	0.12	C
							16.88	0.38	
zq58@1	700	1.86E + 09	3.71E + 06	0.00198835	0.00199828	1.162E − 07	−3.45	0.06	C
zq58@2	700	1.88E + 09	3.74E + 06	0.00198763	0.00199755	1.697E − 07	−3.82	0.08	R
							−3.63	0.26	
zq05@1	800	1.65E + 09	3.31E + 06	0.00201016	0.00202058	1.726E − 07	7.67	0.09	C
zq05@2	800	1.69E + 09	3.40E + 06	0.00200947	0.00201987	1.672E − 07	7.32	0.08	R
							7.49	0.25	
zq18@1	800	1.73E + 09	3.49E + 06	0.00201048	0.00202091	2.433E − 07	7.83	0.12	C
zq18@2	800	1.74E + 09	3.49E + 06	0.00201063	0.00202106	1.683E − 07	7.91	0.08	R
							7.87	0.05	
zq34@1	800	1.70E + 09	3.44E + 06	0.00202749	0.00203795	1.386E − 07	16.33	0.07	R
zq34@2	800	1.73E + 09	3.51E + 06	0.00202671	0.00203715	2.178E − 07	15.93	0.11	C
							16.13	0.28	
zq53@1	800	1.83E + 09	3.65E + 06	0.00198968	0.00199983	1.578E − 07	−2.68	0.08	R
zq53@2	800	1.78E + 09	3.54E + 06	0.00199081	0.00200095	2.086E − 07	−2.12	0.10	R
zq53@3	800	1.89E + 09	3.76E + 06	0.00198920	0.00199933	1.95E − 07	−2.93	0.10	C
zq53@4	800	1.86E + 09	3.70E + 06	0.00198987	0.00200000	1.66E − 07	−2.59	0.08	I
							−2.58	0.34	
zq23@1	850	1.66E + 09	3.35E + 06	0.00201229	0.00202278	1.864E − 07	8.77	0.09	C
zq23@2	850	1.66E + 09	3.34E + 06	0.00201216	0.00202264	1.734E − 07	8.70	0.09	I
zq23@3	850	1.67E + 09	3.37E + 06	0.00201235	0.00202282	1.839E − 07	8.79	0.09	R
							8.75	0.05	
zq66_2@1	875	1.92E + 09	3.83E + 06	0.00198993	0.00199990	2.346E − 07	−2.64	0.12	R
zq66_2@2	875	1.91E + 09	3.80E + 06	0.00198982	0.00199978	2.281E − 07	−2.70	0.11	C
							−2.67	0.04	

zq47@1	900	1.90E + 09	3.78E + 06	0.00199055	0.00200053	2.025E − 07	−2.33	0.10	C
zq65_1@1	900	1.89E + 09	3.76E + 06	0.00199223	0.00200231	1.389E − 07	−1.44	0.07	R
zq65_1@2	900	1.86E + 09	3.70E + 06	0.00199070	0.00200077	1.348E − 07	−2.21	0.07	C
							−1.82	0.54	
zq65_2@1	900	1.87E + 09	3.72E + 06	0.00199201	0.00200208	2.302E − 07	−1.56	0.11	R
zq65_2@2	900	1.88E + 09	3.74E + 06	0.00199088	0.00200094	1.575E − 07	−2.12	0.08	I
zq65_2@3	900	1.88E + 09	3.75E + 06	0.00199077	0.00200081	1.521E − 07	−2.19	0.08	C
zq65_2@4	900	1.88E + 09	3.75E + 06	0.00199241	0.00200245	1.867E − 07	−1.37	0.09	R
zq65_2@5	900	1.91E + 09	3.80E + 06	0.00199096	0.00200097	1.909E − 07	−2.11	0.10	R
zq65_2@6	900	1.90E + 09	3.78E + 06	0.00199112	0.00200113	2.446E − 07	−2.03	0.12	I
							−1.90	0.34	
zq64_1@1	950	1.85E + 09	3.69E + 06	0.00199010	0.00199999	1.815E − 07	−2.60	0.09	R
zq64_1@2	950	1.96E + 09	3.90E + 06	0.00198833	0.00199820	1.479E − 07	−3.49	0.07	C
							−3.05	0.63	
zq64_2@1	950	1.93E + 09	3.84E + 06	0.00198874	0.00199861	2.031E − 07	−3.29	0.10	C
zq64_2@2	950	1.92E + 09	3.83E + 06	0.00198876	0.00199861	2.138E − 07	−3.28	0.11	R
							−3.14	0.00	
zq24@1	1000	1.59E + 09	3.21E + 06	0.00201468	0.00202522	2.604E − 07	9.98	0.13	C
zq24@2	1000	1.58E + 09	3.18E + 06	0.00201536	0.00202589	1.031E − 07	10.32	0.05	I
zq24@3	1000	1.63E + 09	3.29E + 06	0.00201371	0.00202422	1.631E − 07	9.49	0.08	R
							9.93	0.42	
zq36@1	1000	1.79E + 09	3.64E + 06	0.00202963	0.00204002	1.786E − 07	17.37	0.09	C
zq36@2	1000	1.80E + 09	3.65E + 06	0.00202901	0.00203939	2.15E − 07	17.05	0.11	I
zq36@3	1000	1.85E + 09	3.76E + 06	0.00202751	0.00203788	2.598E − 07	16.30	0.13	R
							16.90	0.55	

[a] Corrected for drift and instrumental fractionation.

[b] C = core; I = intermediate; R = rim.

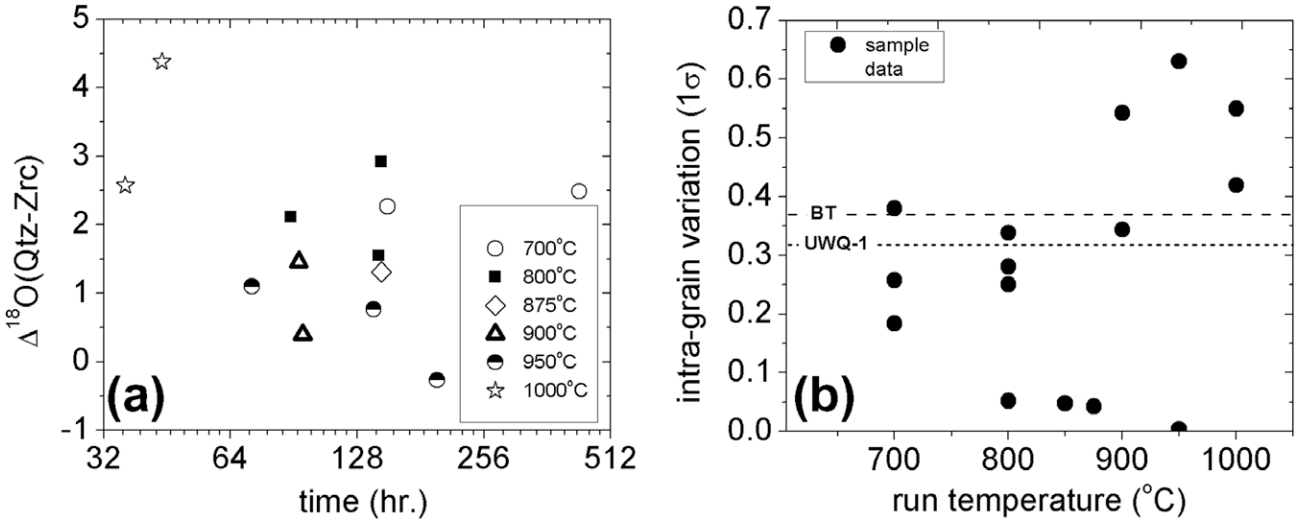

Fig. 3. (a) $\Delta^{18}O$(qtz–zrc) vs. run duration calculated from laser fluorination data. (b) Ion microprobe intra-grain variations for individual grains plotted as a function of crystallization temperature. For comparison, the averages of the ion microprobe standards (BT = Bishop Tuff; UWQ-1 = University of Wisconsin quartz) are included as well. Although the standard deviations calculated in the above plot are based on a small number of analyses, these data seem to indicate larger heterogeneities at higher temperatures; temperatures with the largest intra-grain heterogeneities correlate with the spurious $\Delta^{18}O$(qtz–zrc) values plotted in (a). Grouping multiple grains from single samples together also gives high temperature intra-sample 1σ variations greater than standards.

that calculated deviations are based on a small number of data. That said, the ion microprobe results from the 950 °C experiment suggest *higher* $\delta^{18}O$ values near the grain rim, which would produce A values in better agreement with low temperature results. Moreover, ion microprobe spot data from both 1000 °C grains have *lower* $\delta^{18}O$ values near the rims of grains in both cases, which also would produce A values in better agreement with the lower temperature data. The above observations are surprising, because higher temperature runs are generally considered more likely to reflect equilibrium fractionations. Because of the erratic nature of the higher temperature data, we take this to indicate that these results are unlikely to be reliable; however, some explanation is required.

One possibility is that changes in $\Delta_{qtz-zrc}$ values are related to changes in the oxygen isotope composition of the fluid during crystal growth. As mentioned previously, the hydrothermal fluid (H_2O + dissolved SiO_2) contained 80% of the oxygen in the system, with the remaining 20% divided equally among quartz and zircon synthesis materials. The crystallization of quartz and zircon can be described in broad terms as a fractional Rayleigh condensation reaction. If previously determined α-coefficients for quartz–fluid, and zircon–fluid are applicable (Bottinga and Javoy, 1973; Krylov et al., 2002), and if it is assumed that the mineral fraction reached the maximum value of 20%, then the change from the initial $\delta^{18}O$ water composition can be estimated. With no diffusive equilibration, changes in the fluid composition of ~0.15‰ for temperatures of 700–800 °C are possible; this is consistent with our results given that the measured quartz and zircon $\delta^{18}O$ values bracket the initial $\delta^{18}O$ water values of the experiments (Table 1 and EA-4). This very small difference is related to estimated $\alpha_{mineral-H2O}$ coefficients of zircon (1.006 at 800 °C) and quartz (0.993 at 800 °C) acting in a somewhat compensatory fashion, mitigating against changes in the oxygen isotope composition of the fluid. However, if $\alpha_{mineral-H2O}$ values change with higher dissolved SiO_2 contents (i.e., at higher temperatures), this may lead to appreciable changes in the fluid composition, especially if both α-coefficients become greater or less than one. This seems plausible, especially since the high-temperature data (e.g., zq43, 44, 52, 61, 64, 66) have final quartz and zircon values that do not bracket the initial water value. For example, if the initial water and final mineral values are used to approximate $\alpha_{mineral-H2O}$ coefficients in the two most extreme cases (zw61, $T = 950$ °C; zw44, $T = 1000$ °C), a Rayleigh condensation calculation suggests a change in the final H_2O value of 0.9‰ and 0.7‰, respectively. While there are no quartz–fluid studies characterizing the fractionation behavior related to salt effects at temperatures greater than 800 °C, (Clayton et al., 1972; Bottinga and Javoy, 1973; Matsuhisa et al., 1979), fractionation reversals in mineral–fluid systems are plausible in this temperature range (Bottinga and Javoy, 1973; Schütze, 1980; Matthews et al., 1983a,b; Chacko et al., 2001). It is also possible that one mineral may have crystallized or recrystallized at different times from the other; this process has in the past been used to explain discrepancies between experimental and natural calibrations (Sharp and Kirschner, 1994).

Another alternative is that the surface $\delta^{18}O$ value of a crystal in equilibrium with a fluid may have a different $\delta^{18}O$ value than the lattice in equilibrium with the same fluid (Onasch and Vennemann, 1995; Watson and Liang, 1995; Watson, 2004). If a difference does exist, and if mineral growth rates are fast enough to incorporate the surface oxygen isotope "equilibrium" composition into the lattice, then this would affect measured fractionations. While both quartz and zircon may be susceptible to this process, the possibility seems more probable for quartz based on a

couple observations. First, oxygen data collected in a silica undersaturated hydrothermal system showed no variation in zircon–fluid values vs. time over the same temperature range explored here (Krylov et al., 2002). Second, this process has been documented for quartz grains in natural samples (Onasch and Vennemann, 1995). In order to quantify this behavior, as discussed by Watson and Liang (1995), the thickness of the surface layer must be known, as well as partition coefficients between surface and fluid which is at least a function of temperature and composition.

In certain cases—while contrary to expectation—the attainment of equilibrium is not necessarily favored by higher temperatures. We suspect that one or both of the possibilities suggested above are responsible for the observed high temperature features, but available parameters necessary for additional calculation are unavailable, meaning our analysis falls well short of proof.

4.2. Preferred quartz–zircon fractionation values

Data collected from 700 to 875 °C were included in our final calibration because no time dependence of $\Delta_{qtz-zrc}$ values was apparent, and because ion microprobe data yielded low standard deviations for individual grains. The 20 kbar, 900 °C run was included because grains were small enough to equilibrate diffusively (Farver and Yund, 1991). Laser fluorination data for quartz from zq43 (900 °C, 10 kbar), produced an error about twice as large as those determined from quartz of other runs, and is in excess of two standard deviations from the reproducibility of the standards. This suggests that the variability among $\delta^{18}O$ values in quartz grains is true inter-grain heterogeneity. Moreover, the ion microprobe data gave poor intra-grain reproducibility for a 900 °C, 10 kbar run, possibly indicating oxygen isotope zoning. On the basis of these lines of evidence, our preferred calibration does not include zq43. The data from experiments at 950–1000 °C are also not included because of the observed time dependence of the $\Delta_{qtz-zrc}$ values for 950 °C runs, and the intra-grain variability of the ion microprobe data shown in Fig 3b. Negative $\Delta_{qtz-zrc}$ values (i.e., zq64) are in disagreement with first-principle models of oxygen isotope fractionations; the small size and high ionic potential of Si^{4+} is predicted to preferentially incorporate ^{18}O relative to the larger Zr^{4+}, which has lower vibrational frequencies (Kieffer, 1982). Finally, if salt effects are limited, then quartz should be higher than the $\delta^{18}O$ value of the starting water and the zircon should be lower. However, for the high-T runs with larger standard deviations, this is never the case, and can be taken as another line of evidence that these data are less reliable.

Our preferred calibration therefore includes data from temperatures ranging from 700 to 900 °C and pressures of 10 and 20 kbar, covering a P–T range directly applicable to natural systems. These data are plotted in Fig. 4 as $1000\alpha_{qtz-zrc}$ vs. $1/T^2$ (in K) and regressed through the origin based on the assumption that $\Delta_{qtz-zrc} \to 0$ as $T \to \infty$. The A value calculated on the basis of the selected data set is 2.33 ± 0.24. Note however, that if all data from Table 1 are included in the fit, the resulting A value is 2.24 ± 0.42. These values are the same within error, but for reasons discussed above, not all data are considered equally reliable.

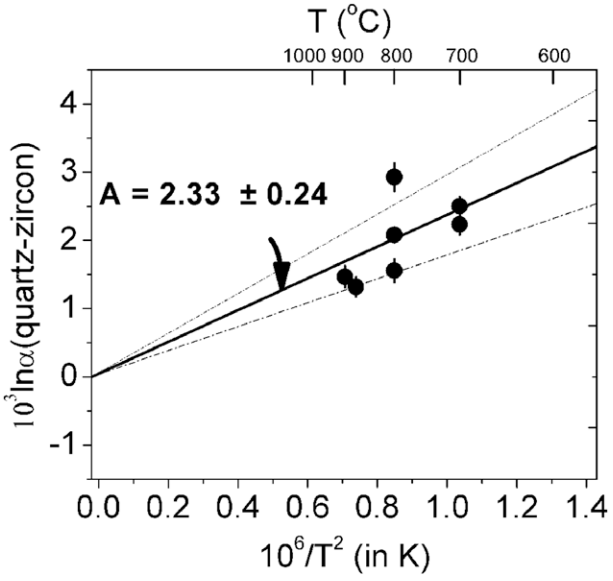

Fig. 4. 1000 ln α(quartz–zircon) vs. $10^6/T^2$, where each data point represents an individual run. Linear regression gives an A value of 2.33 ± 0.24. The dashed lines indicate 95% confidence intervals.

4.3. Comparison with other zircon fractionation factors

Here, we discuss theoretical, empirical, and experimental studies that have led to fractionation factors for zircon. The theoretical calibration of Kieffer (1982) used the vibrational spectra of ^{16}O minerals, and applied a set of rules to calculate the shift factor for ^{18}O substitution. This calibration gives $A_{qtz-zrc} = 3.0$.

Semi-empirical calibrations are generally based upon observations and results from experimental and natural data. For example, it was first noted that minerals with stronger bonds such as Si–O also have higher relative $\delta^{18}O$ values (Taylor and Epstein 1962a,b). This was subsequently extended by Garlick (1966), and later Schütze (1980) developed the increment method to approximate fractionation factors for minerals. The increment method calculates fractionation factors based on differences in cation mass and bond strengths relative to a well-characterized reference phase; this technique was later modified by Zheng (1991). A version of the increment method was applied by Hoffbauer et al. (1994) to determine the reduced partition function ratio (β-factor) for the reference phase quartz. This was calculated using mineral–calcite experimental data (Clayton et al., 1989; Chiba et al., 1989), in addition to their calculated index value for anorthite which implied $A_{qtz-zrc} = 2.06$. However, using a more commonly accepted β-factor for quartz gives $A_{qtz-zrc} = 3.25$ (Zheng, 1993). Finally, Smyth (1989) determined the mean electrostatic potentials of oxygen sites in quartz and zircon; the empirical 1000 ln $\alpha_{qtz-mineral}$ vs. $\Delta_{site\ potential}$ relationship discussed in Chacko et al. (2001) can be used to calculate $A_{qtz-zrc} = 3.18$.

Calibrations are also possible from measurements on natural materials with careful selection of sample material, but require an independent thermometer which may be

inaccurate, and equilibrium $\delta^{18}O$ values can not be guaranteed. In addition, the slow kinetics of zircon dissolution in crustal melts means that the analysis of inherited grains are possible (Watson, 1996). An indirect empirical calibration was derived by measuring oxygen isotope fractionation between zircon and titanite, which produced an implied $A_{qtz-zrc}$ value of 2.55 (King et al., 2001). A direct empirical calibration from the Bishop Tuff magma body constrained by quartz–magnetite isotope fractionations and Fe–Ti oxide temperatures (Hildreth, 1979) also produced $A_{qtz-zrc} = 2.55$ (Bindeman and Valley, 2002); in addition, a calibration was determined from multiple felsic volcanic rocks suggesting $A_{qtz-zrc} = 2.64$ (Valley et al., 2003).

Two previous experimental studies are in sharp contrast with theoretical and natural studies. Krylov et al. (2002) relied on the expectation that independent quartz–water equilibrium experiments and zircon–water experiments could be combined to predict a quartz–zircon fractionation factor. This meant that calculation of $A_{qtz-zrc}$ required selection of an additional quartz–water fractionation factor which may influenced by salt effects (Hu and Clayton, 2003). Second, selection of a quartz–water fractionation data set is not necessarily straightforward since these calibrations are somewhat variable (e.g. Clayton et al., 1972; Bottinga and Javoy, 1973; Matsuhisa et al., 1979). Using the quartz–H_2O fractionation data of Bottinga and Javoy (1973), Krylov et al. (2002) calculated $A_{qtz-zrc} = 1.36$. Another experimental study based on isotope exchange between zircon and calcite suggested a negative $A_{qtz-zrc}$ value (Sessions et al., 1996).

While our experimental results are in broad agreement with the calibrations from natural samples, most semi-empirical and theoretical $A_{qtz-zrc}$ values derived using different methods converge to a value of ~3.1 (Kieffer, 1982; Smyth, 1989; Zheng, 1993). Since this is statistically resolvable from our preferred experimental calibration as well as natural calibrations, modeling performed in Section 5.2 include calculations with experimental and theoretical A-values for comparison with natural data.

5. GEOCHEMICAL APPLICATIONS

The calibration of an oxygen isotope fractionation factor for zircon will be useful in assessing equilibrium/disequilibrium in rocks, and may help to distinguish igneous from metamorphic or hydrothermal processes. For example, even if the matrix of the rock is completely altered, as is the case with bentonites, zircon $\delta^{18}O$ values (and possibly quartz) may provide information about the $\delta^{18}O$ value of an ancient volcanic eruption, even in hydrothermally altered and re-melted rocks (e.g., Bindeman et al., 2008). Zircon will also be less susceptible to isotope exchange during protracted cooling events; this effect may be further mitigated—although not necessarily eliminated—if *in situ* techniques are used to target zircon cores. In this section, equilibrium calculations of mineral–zircon and melt–zircon fractionations are presented, which are applicable to a wide variety of systems, provided zircon can be assumed not to have been compromised by post crystallization exchange.

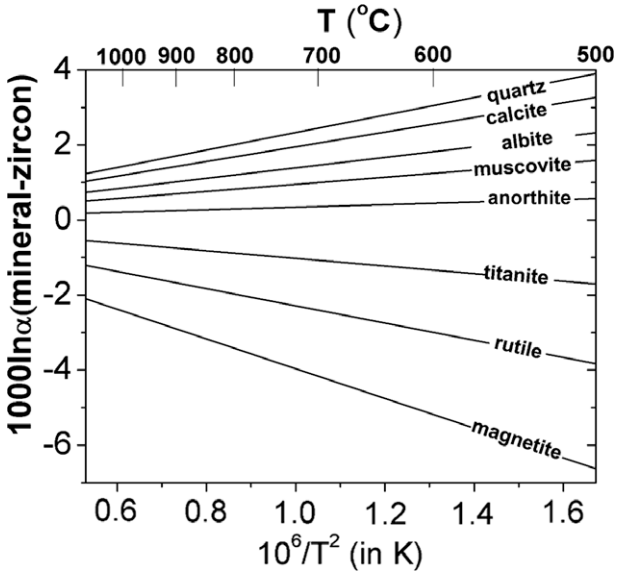

Fig. 5. Mineral–zircon oxygen fractionations vs. temperature, over geologically relevant conditions. Fractionations are included for quartz (see Section 4), calcite (Clayton et al., 1989), albite (Clayton et al., 1989), muscovite (Chacko et al., 1996), anorthite (Clayton et al., 1989), titanite (King et al., 2001), rutile (Chacko et al., 1996), and magnetite (Chiba et al., 1989).

5.1. Mineral–zircon oxygen isotope fractionations

Calculated oxygen isotope fractionations between zircon and other rock-forming minerals vs. temperature are plotted in Fig. 5 with $A_{qtz-zrc} = 2.33$. Zircon is generally depleted in ^{18}O relative to rock-forming silicates common among crustal rocks. In addition, as expected, Ti and Fe oxides are depleted in ^{18}O relative to zircon. If oxygen isotope measurements from these minerals are combined with other thermometers—especially those that are that are complementary to zircon (e.g., Watson et al., 2006; Hayden et al., 2007)—processes bearing on rock and mineral formation can be further explored. The direct application of Fig. 5 implies the same oxygen closure temperatures of the mineral pairs, which is generally not the case. Since the closure temperature of zircon is higher than other minerals, the complementary mineral will likely continue to exchange oxygen at lower temperatures (e.g., Eiler et al., 1993; Kohn and Valley, 1998). Thus, it is not surprising that quartz–zircon oxygen isotope fractionations can sometimes produce "temperatures" lower than expected, especially for plutonic rocks (e.g., Lackey et al., 2008).

5.2. Calculation of WR/melt–zircon oxygen isotope fractionations

Various functions have been fit to natural data that suggests a higher whole rock (WR) silica content leads to larger Δ_{WR-zrc} values (e.g., Valley et al., 1994, 2005; Lackey et al., 2008). For example, Lackey et al. (2008) showed that Δ_{WR-zrc} values vary in a broadly linear fashion with SiO_2 content. Values of 0.3‰, and 2.1‰ for 45 to 75 wt.% SiO_2 rock

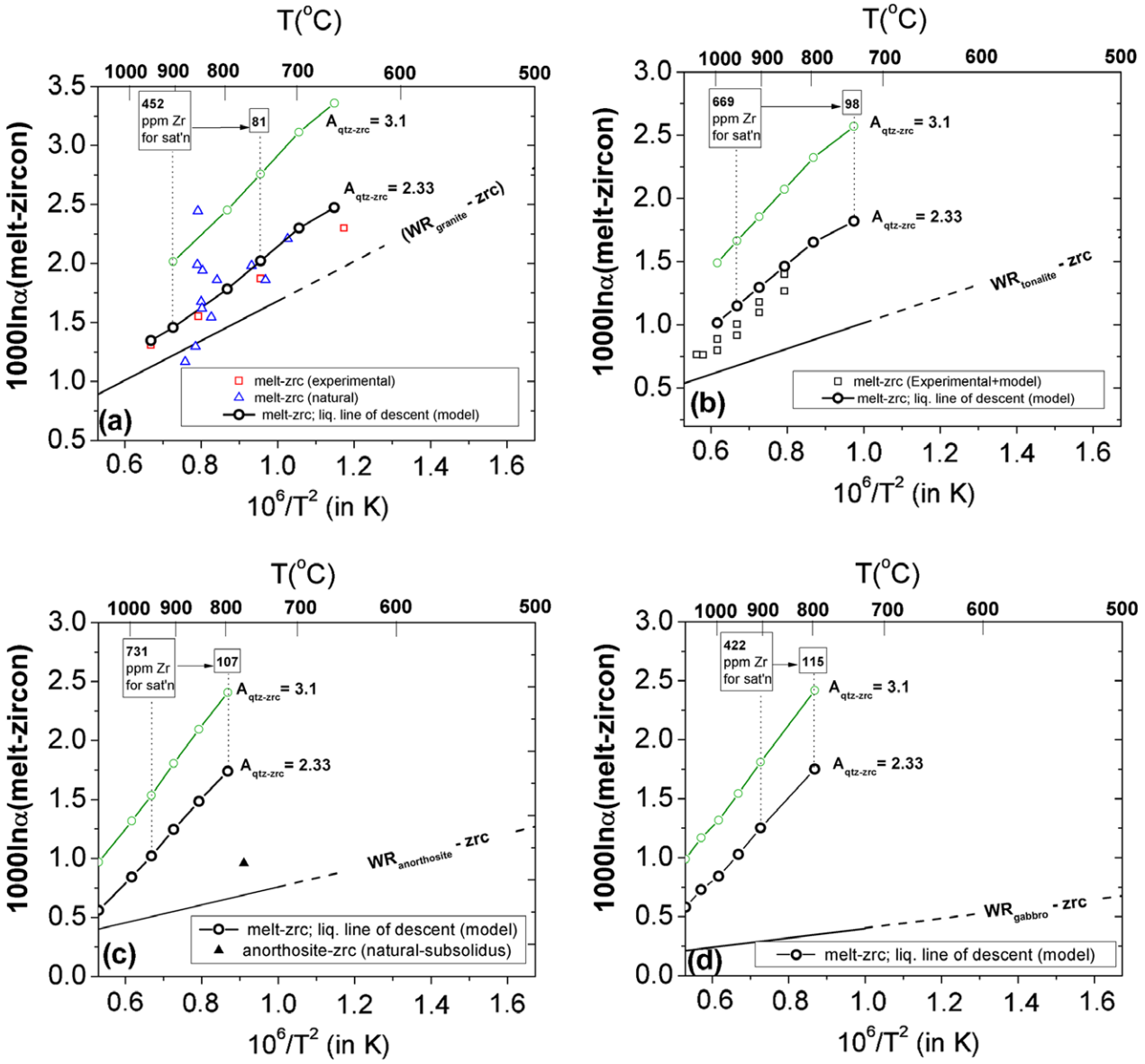

Fig. 6. Calculated oxygen isotope fractionations between WR/melt and zircon. The WR–zircon fractionation lines ($A_{qtz–zrc} = 2.33$) are valid if WR and zircon have completely re-equilibrated at subsolidus temperatures. The melt–zircon fractionations are calculated based on the chemistry of the remaining melt as determined by the MELTS algorithm and the model presented in Section 5.2 and EA-6 for oxygen isotope fractionation in melts. For comparison, melt–zircon fractionations are plotted with $A_{qtz–zrc} = 2.33$ and the best estimate from theoretical studies. ($A_{qtz–zrc} = 3.1$). (a) Rhyolite melt–zircon fractionations; host melt is from sample 99LV-751, Bindeman and Valley (2002). Model melt–zircon fractionations are larger than WR–zircon fractionations; this trend agrees well with data from natural samples (Bindeman and Valley, 2001, 2002) and with experimental data calculated from Rhyolite–CO_2 and silica–CO_2 fractionation studies (Matthews, 1994; Palin et al., 1996). In addition, our experimental fractionation factor for zircon is in better agreement with natural data than that predicted from most theoretical calculations. (b) Tonalite WR/melt–zircon evolution using "Tonalite 101" composition from Carroll and Wyllie (1989) and $A_{qtz–zrc} = 2.33$. Calculated MELTS algorithm compositions vs. T agree well with experimental results from Carroll and Wyllie (1989); melt–zircon fractionations from these two data sets are only marginally different. (c) Anorthosite host rock (Le Maitre, 1976; reproduced in EA-5). (d) Average gabbro host rock using the composition found in Le Maitre (1976). Of the four host rock case studies, gabbros produce the largest WR–zircon vs. melt–zircon fractionation differences because a gabbro undergoes the largest change in melt chemistry during crystallization.

content were measured, respectively, along with all values in between for samples from the Central Sierra Nevada Batholith. Here we model $\Delta_{WR/melt–zrc}$ values for compositions equivalent to rhyolite, tonalite, gabbro, and anorthosite with WR SiO_2 contents from 76 to 51 wt.% (EA-5).

First, the melt composition was determined along a liquid line of descent with the MELTS algorithm at constant pressure for each of the four rock types (Ghiorso and Sack, 1995; Asimow and Ghiorso, 1998). Second, melt–zircon fractionation factors were determined through general

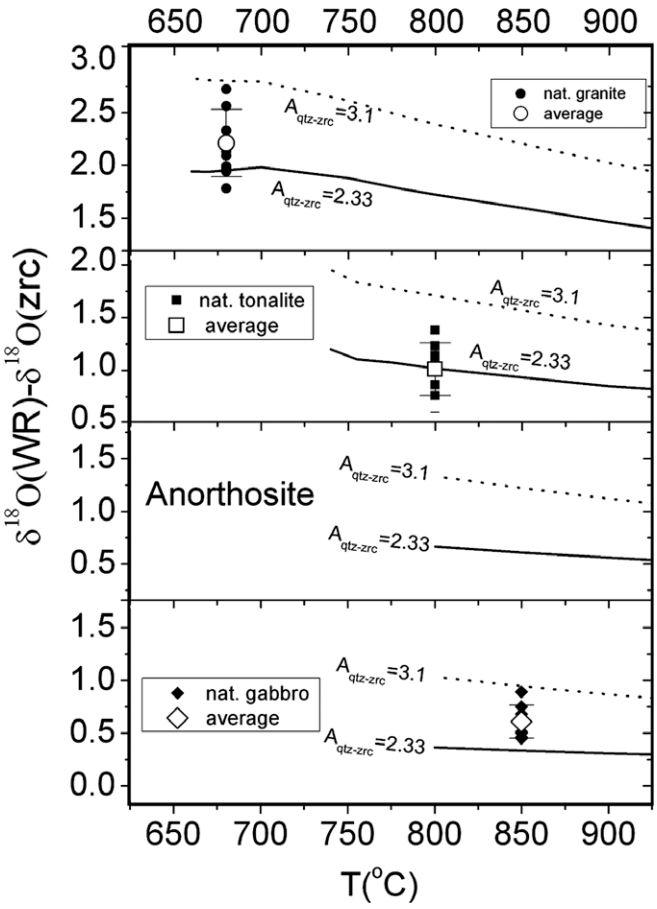

Fig. 7. Predicted $\Delta_{WR-zircon}$ values from the four case study rocks (EA-5), taking into consideration that the melt composition (and $\delta^{18}O$ value) during crystallization will not be the same as the WR composition. The model is reproduced with our experimental fractionation factor and average fractionation factor calculated from experimental studies. Assuming our model is correct, the theoretical fractionation factor for zircon always overestimates $\Delta_{WR-zircon}$ when compared to natural data taken from Lackey et al. (2008). Natural rocks were selected based on similar WR SiO_2 compositions to those in EA-5. Crystallization temperatures for natural data are estimated according to the protocol outlined by Lackey et al. (2008).

application of the model of Zhao and Zheng (2003); we additionally took into account a ~3.5% increase in the reduced partition function ratio of silica glass relative to quartz. That is, at equilibrium, silica glass is enriched in ^{18}O relative to quartz (Stolper and Epstein, 1991; Clayton and Kieffer, 1991; Matthews et al., 1994). The application of MELTS also allowed us to estimate the value of the melt compositional parameter '*M*' defined in Watson and Harrison (1983), which can be used to calculate the concentration of zirconium necessary for zircon saturation in a given melt. Further details of the model applied and calculations performed can be found in EA-6.

5.2.1. Model results

The initial host–rock compositions, representative melt vs. temperature calculations, and other model parameters can be found in EA-5. The calculated WR–zircon and melt–zircon fractionations are shown in Fig. 6 using $A_{qtz-zrc=}2.33$ and 3.1, along with natural data for comparison. The WR–zircon fractionation lines represent the case of subsolidus equilibration between WR and zircon in a closed system. The melt–zircon fractionations are most appropriately applied to volcanic rocks, and the plutonic case will be discussed later since it builds upon the results in Fig. 6.

More evolved melts and late-stage mafic melt residuals produce the largest melt–zircon fractionations. Fig. 6 also implies fractionation between the melt and crystallized fraction will be positive at equilibrium; that is, the melt $\delta^{18}O$ value will be higher than the crystallized fraction. This is expected since it has been known for some time that mafic minerals have low $^{18}O/^{16}O$ ratios and tend to crystallize early, leaving the melt not only more polymerized but also with a higher $\delta^{18}O$ value (e.g., Taylor and Epstein, 1962a,b). While the $\Delta_{melt-zrc}$ fractionations are larger than Δ_{WR-zrc} in all cases, the magnitudes of these differences depend upon the rock type and resulting melt, and are discussed below. These graphs also include the estimated Zr concentration required for zircon saturation given the melt composition at that temperature (EA-5).

From the four rocks examined, the rhyolite contained the smallest fractionation differences between melt and WR at a given temperature. For example, at 700 °C the $\Delta_{melt-zrc}$ fractionation is 2.2 vs. a Δ_{WR-zrc} value of 1.8 using

$A_{qtz-zrc} = 2.33$. This is expected because melts of rhyolitic composition crystallize over a relatively restricted temperature range, leading to comparatively small changes in the melt composition. If the assumptions of this model are valid (EA-6), our experimental fractionation factor for zircon is in better agreement with natural melt–zircon data than the theoretical fractionation factor.

Much larger changes in melt compositions and $\delta^{18}O$ values are observed for intermediate and more mafic rocks. For example, using the WR tonalite data from an experimental study (Tonalite 101; Carroll and Wyllie, 1989), Fig. 6b shows the Δ_{WR-zrc} and $\Delta_{melt-zrc}$ fractionations deviate at lower temperatures and higher SiO_2 content. Carroll and Wyllie (1989) experimentally determined melt composition vs. temperature; therefore, their chemical melt data can be used to directly calculate melt–zircon fractionations. These results are in good agreement with $\Delta_{melt-zrc}$ fractionations calculated from melt compositions derived from MELTS. Increasing melt–zircon fractionation factors with decreasing temperature are also predicted for the anorthosites and gabbros.

Lastly, in order to directly calculate the final WR–zircon value for plutonic rocks (WR–zircon fractionations in Fig. 6 are for subsolidus exchange), melt–zircon fractionations at the time of zircon crystallization must be known (EA-5 and Fig 6). Also, the zircon $\delta^{18}O$ value will depend on the absolute $\delta^{18}O$ value of the melt at the time of crystallization. Using the technique described in EA-6, WR–zircon values are calculated using the experimental and theoretical zircon fractionation factors, and are presented along with some natural WR–zircon data for comparison (Fig. 7). Results are in closest agreement with natural data if an $A_{qtz-zrc}$ value of 2.33 is used (vs. $A_{qtz-zrc} = 3.1$); on average Δ_{WR-zrc} natural data are $\sim$0.2Δ-units higher than model prediction, which is within the uncertainty of our calibration. Application of the model using the theoretical fractionation factor for zircon produces values $\sim$0.6Δ-units lower than natural data.

Overall, Δ_{WR-zrc} estimations calculated from melt–zircon fractionation factors do not vary substantially from the subsolidus Δ_{WR-zrc} fractionations presented in Fig 6. Even though a late-stage mafic melt fraction becomes enriched in ^{18}O, as shown here and by other workers (e.g., Bindeman et al., 2004), it does not lead to higher absolute $\delta^{18}O$ values for zircon, because the melt–zircon fractionation factor also increases. For example, if the WR initial value of the gabbro presented in EA-5 is +6‰, then at 850 °C the calculated $\delta^{18}O$ value of the remaining melt is $\sim$7.2‰. The $A_{melt-zrc}$ value at 850 °C is $\sim$1.9 (using $A_{qtz-zrc} = 2.33$), meaning that the zircon will crystallize (if saturation has been reached) with a $\delta^{18}O$ value of approximately +5.2‰.

While the model is better agreement with natural observations if the experimental fractionation factor is used, this no way proves that the theoretical studies are incorrect. Furthermore, this should not be taken as a line of evidence that our experiments demonstrate equilibrium. Our A-value (or those derived from natural studies) simply produces the best agreement with natural $\Delta_{melt-zircon}$ and $\Delta_{WR-zircon}$ data, though there are uncertainties involved in this calculation. For example, the zircon crystallization temperature of natural samples may be variable; this was confirmed by Harrison et al. (2007) who showed that zircons from tonalitic melts can crystallize over a 125 °C temperature range. Second, while simplifying the calculation, the assumption of a closed WR may not be valid, and zircon may also have been disturbed after crystallization. Finally, so that simple comparisons could be made, the natural rocks selected for comparison in Fig 7 were of similar SiO_2 content, but not of identical composition to the four "case study" rocks presented in EA-5.

Nonetheless, if the above methods are combined with a thermometer, and $\delta^{18}O$ values for zircon and WR are known, this may help to access whole rock or zircon hydrothermal alteration (King et al., 1997; Hoskin, 2005). In addition, one common application for the study of oxygen isotopes in zircon is aimed at constraining the provenance of grains no longer associated with their host rocks (e.g., Mojzsis et al., 2001; Wilde et al., 2001; Valley et al., 2005; Cavosie et al., 2005; Trail et al., 2007). The direct application of the above model will require some estimation of the melt composition, and an estimation of the zircon crystallization temperature. If the assumptions of the Ti-in-zircon thermometer hold (Watson et al., 2006; Ferry and Watson 2007; Hofmann et al., 2009) and other lines of evidence such as inclusion mineralogy are available (e.g., Hopkins et al., 2008), source melt oxygen isotope compositions can be reasonably constrained. For example, if quartz inclusions are found (i.e., SiO_2 saturated rocks), and if the zircon crystallized at $\sim$700 °C, the $\delta^{18}O$ value of the WR is very likely to be $\sim$1.3 to 2.0‰ higher than measured zircon values; this result derived from the model presented above is in excellent agreement with the natural measurements made by Lackey et al. (2008).

6. CONCLUDING REMARKS

We have reported the first direct experimental calibration for oxygen isotope fractionation between quartz and zircon. Hydrothermal experiments interpreted to represent the best experimental estimate of an A value to-date included experiments from 700 to 900 °C. Pressure and fO_2 appear to have no measurable effect on the fractionation factor. Time-dependent variations in $\Delta_{qtz-zrc}$ were measured for higher temperature runs, and ion microprobe data appear to contain larger intra-grain deviations at higher temperature as well. Our preferred calibration is broadly consistent with those based on natural data (King et al., 2001; Bindeman and Valley, 2002; Valley et al., 2003), is lower than most theoretical and semi-empirical calculations (cf. Hoffbauer et al., 1994), but contrasts sharply with past experimental work. The results presented here help to eliminate some of the uncertainty that arose from previous experimental calibrations.

Since zircon is among the least susceptible crustal minerals to diffusive exchange, it may be the most likely to preserve equilibrium oxygen isotope compositions reflecting conditions of crystallization. A zircon fractionation factor can therefore be robustly applied to petrogenetic problems, equilibrium oxygen isotope compositions of co-existing

minerals, and may help to characterize zircon source melts. To illustrate this, mineral–zircon and melt–zircon fractionations were calculated as a function of temperature; results show that zircon is among the most depleted ^{18}O mineral of common crustal silicates, and that the composition of the melt affects $\Delta_{melt-zrc}$. Calculations suggest that the final measured zircon $\delta^{18}O$ value can be influenced by the rock type, the zircon saturation temperature, melt–zircon fractionations, and the absolute value of the melt.

Model results show an A value of 2.33 (or A values from natural calibrations) produce results that are in better agreement with natural $\Delta_{WR/melt-zircon}$ data than theoretical fractionation factors for zircon. Based on experiments and models presented here, fundamental arguments based on oxygen isotopes in zircon now stand on firmer ground.

ACKNOWLEDGMENTS

This work was supported by NSF Grant No. EAR-0440228 to E.B. Watson and the ion microprobe facility at UCLA is partly supported by a grant from the Instrumentation and Facilities Program, Division of Earth Sciences, National Science Foundation. Laser fluorination analyses at Univ. of Oregon were supported by NSF Grant No. EAR-0844772. We thank J.W. Valley, two anonymous reviewers, and the handling editor, T. Chacko for many helpful suggestions that greatly improved the manuscript.

APPENDIX A. SUPPLEMENTARY DATA

Supplementary data associated with this article can be found, in the online version, at doi:10.1016/j.gca.2009.08.024.

REFERENCES

Asimow P. D. and Ghiorso M. S. (1998) Algorithmic modifications extending MELTS to calculate subsolidus phase relations. *Am. Min.* **83**, 1127–1131.

Bindeman I. N. and Valley J. W. (2001) Low-$\delta^{18}O$ rhyolites from yellowstone: magmatic evolution based on analyses of zircon and individual phenocrysts. *J. Petrology* **42**, 1491–1517.

Bindeman I. N. and Valley J. W. (2002) Oxygen isotope study of the long Valley–Glass Mountain magmatic system, California: isotope thermometry, and the convection in large silicic magma bodies. *Contrib. Mineral. Petrol.* **144**, 185–205.

Bindeman I. N., Ponomareva V. V., Bailey J. C. and Valley J. W. (2004) Volcanic arc of Kamchatka: a province with high-$\delta^{18}O$ magma sources and large-scale $^{18}O/^{16}O$ depletion of the upper crust. *Geochim. Cosmochim. Acta* **68**, 841–865.

Bindeman I. N., Fu B., Kita N. and Valley J. W. (2008) Origin and evolution of Yellowstone silicic magmatism based on ion microprobe analysis of isotopically-zoned zircons. *J. Petrology* **49**, 163–193.

Bottinga Y. and Javoy M. (1973) Comments on oxygen isotope geothermometry. *Earth Planet. Sci Lett.* **20**, 250–265.

Cavosie A. J., Valley J. W., Wilde S. A. and Edinburg Ion Microphone Facility (2005) Magmatic $\delta^{18}O$ in 4400–3900 Ma detrital zircons: A record of the alteration and recycling of crust in the early Archean. *Earth Planet. Sci. Lett.* **235**, 663–681.

Carroll M. R. and Wyllie P. J. (1989) Experimental phase relations in the system tonalite–peridotite–H_2O at 15 kb: Implications for assimilation and differentiation processes near the crust–mantle boundary. *J. Petrology* **30**, 1351–1382.

Chacko T., Cole D. R. and Horita J. (2001) Equilibrium oxygen, hydrogen and carbon isotope fractionation factors applicable to geologic systems. *Rev. Min.* **43**, 1–81.

Chacko T., Hu X. S., Mayeda T. K., Clayton R. N. and Goldsmith J. R. (1996) Oxygen isotope fractionations in muscovite, phlogopite, and rutile. *Geochim. Cosmochim. Acta*, **60** 2595–2608.

Chiba H., Chacko T., Clayton R. N. and Goldsmith J. R. (1989) Oxygen isotope fractionations involving diopside, forsterite, magnetite, and calcite: application to geothermometry. *Geochim. Cosmochim. Acta* **53**, 2985–2995.

Cherniak D. J. (2008) Si diffusion in zircon. *Phys. Chem. Mater.* **35**, 179–187.

Clayton R. N., O'Neil J. R. and Mayeda T. K. (1972) Oxygen isotope exchange between quartz and water. *J. Geophys. Res.* **77**, 3057–3067.

Clayton R. N., Goldsmith J. R. and Mayede T. K. (1989) Oxygen isotope fractionation in quartz, albite, anorthite, and calcite. *Geochim. Cosmochim. Acta.* **53**, 725–733.

Clayton R. N. and Kieffer S. W. (1991) Oxygen isotopic thermometer calibrations. In: *Stable isotope geochemistry: A tribute to Samuel Epstein* (ed. H. P. Taylor et al.) *Geochem Soc Spec Publ. No*. **3**, 3–10.

Downs W. F., Touysinhthiphonexay Y. and Deines P. (1981) A direct determination of the oxygen isotope fractionation between quartz and magnetite at 600 and 800 °C and 5 kbar. *Geochim. Cosmochim. Acta* **45**, 2065–2072.

Eiler J. M., Valley J. W. and Baumgartner L. P. (1993) A new look at stable isotope thermometry. *Geochim. Cosmochim. Acta* **57**, 2571–2583.

Farver J. R. and Yund R. A. (1991) Oxygen diffusion in quartz: dependence on temperature and water fugacity. *Chem. Geol.* **90**, 55–70.

Ferry J. M. and Watson E. B. (2007) New thermodynamic models and revised calibrations for the Ti-in-zircon and Zr-in-rutile thermometers. *Contrib. Mineral. Petrol.* **154**, 429–437.

Garlick G. D. (1966) Oxygen isotope fractionation in igneous rocks. *Earth Planet. Sci. Lett.* **1**, 361–368.

Ghiorso M. S. and Sack R. O. (1995) Chemical mass transfer in magmatic processes. IV. A revised and internally consistent thermodynamic model for the interpolation and extrapolation of liquid–solid equilibria in magmatic systems at elevated temperatures and pressures. *Contrib. Mineral. Petrol.* **119**, 197–212.

Harrison T. M., Blichert-Toft J., Müller W., Albarède F., Holden P. and Mojzsis S. J. (2005) Heterogeneous Hadean hafnium: evidence of continental crust at 4.4–4.5 Ga. *Science* **310**, 1947–1950.

Harrison T. M., Watson E. B. and Aikman A. B. (2007) Temperature spectra of zircon crystallization in plutonic rocks. *Geology* **35**, 635–638.

Hayden L. A., Watson E. B. and Wark D. A. (2007) A thermobarometer for sphene (titanite). *Contrib. Mineral. Petrol.* **155**, 529–540.

Hildreth W. (1979) The Bishop Tuff: evidence for the origin of compositional zonation in silicic magma chambers. In: Chapin, C.E. & Elston, W. E. (eds) *Ash-flow tuffs. Geological Society of America, Special Paper* 180:43–75.

Hofmann A. E., Valley J. W., Watson E. B., Cavosie A. J. and Eiler J. M. (2009) Sub-micron scale distributions of trace elements in zircon. *Contrib. Mineral. Petrol.* **158**, 317–355.

Hoffbauer R., Hoernes S. and Fiorentini E. (1994) Oxygen isotope thermometry based on a refined increment method and its

application to granulite-grade rocks from Sri Lanka. *Precamb. Res.* **66**, 199–220.

Hopkins M., Harrison T. M. and Manning C. M. (2008) Low Heat Flow inferred from >4 Gyr zircons suggests Hadean plate boundary interactions. *Nature* **456**, 493–496.

Hoskin P. W. O. (2005) Trace-element composition of hydrothermal zircon and the alteration of Hadean zircon from the Jack Hills, Australia. *Geochim. Cosmochim. Acta* **69**, 637–648.

Hu G. X. and Clayton R. N. (2003) Oxygen isotope salt effects at high pressure and high temperature and the calibration of oxygen isotope geothermometers. *Geochim. Cosmochim. Acta* **67**, 3227–3246.

Kieffer S. W. (1982) Thermodynamics and lattice vibrations of minerals: 5. Applications to phase equilibria, isotopic fractionation, and high-pressure thermodynamic properties. *Rev. Geophys. Space Phys.* **20**, 827–849.

Kelly J. L., Fu B., Kita N. T. and Valley J. W. (2007) Optically continuous silcrete quartz cements of the St. Peter Sandstone: High precision oxygen isotope analysis by ion microprobe. *Geochim. Cosmochim. Acta* **71**, 3812–3832.

King E. M., Barrie C. T. and Valley J. W. (1997) Hydrothermal alteration of oxygen isotope ratios in quartz phenocrysts, Kidd Creek mine, Ontario: magmatic values are preserved in zircon. *Geology* **25**, 1079–1082.

King E. M., Valley J. W., Davis D. W. and Kowallis B. J. (2001) Empirical determination of oxygen isotope fractionation factors for titanite with respect to Zircon and Quartz. *Geochim. Cosmochim. Acta* **65**, 3165–3175.

Kohn M. J. and Valley J. W. (1998) Obtaining equilibrium oxygen isotope fractionations from rocks: theory and examples. *Contrib. Miner. Petrol.* **132**, 209–224.

Krylov D.P., Zagnitko V.N., Hoernes S., Lugovaja I.P. and Hoffbauer R. (2002) Oxygen isotope fractionation between zircon and water: experimental determination and comparison with quartz–zircon calibrations. *Eur. J. Min.* **14** 849–853.

Lackey J.S., Valley J.W., Chen J.H. and Stockli D.F. (2008) Dynamic magma systems, crustal recycling, and alteration in the central Sierra Nevada batholith: the oxygen isotope record. *J. Petrology* **49** 1397–1426.

Le Maitre R. W. (1976) The chemical variability of some common magmatic rocks. *J. Petrology* **17**, 589–637.

Manning C. E. (1994) The solubility of quartz in H_2O in the lower crust and upper mantle. *Geochim. Cosmochim. Acta* **57**, 1079–1091.

Matthews A., Goldsmith J. R. and Clayton R. N. (1983a) Oxygen isotope fractionation involving pyroxenes: the calibration of mineral-pair geothermometers. *Geochim. Cosmochim. Acta* **47**, 631–644.

Matthews A., Goldsmith J. R. and Clayton R. N. (1983b) Oxygen isotope fractionation between zeolite and water. *Geochim. Cosmochim. Acta* **47**, 645–654.

Matthews A. (1994) Oxygen isotope geothermometers for metamorphic rocks. *J. Metamorphic Geol.* **12**, 211–219.

Matthews A., Palin J. M., Epstein S. and Stolper E. M. (1994) Experimental study of $^{18}O/^{16}O$ partitioning between crystalline albite, albite glass, and CO_2 gas. *Geochim. Cosmochim. Acta* **58**, 5255–5266.

Matsuhisa Y., Goldsmith J. R. and Clayton R. N. (1978) Methods of hydrothermal crystallization of quartz at 250 °C and 15 kbar. *Geochim. Cosmochim. Acta* **42**, 173–182.

Matsuhisa Y., Goldsmith J. R. and Clayton R. N. (1979) Oxygen isotopic fractionation in the system quartz–albite–anorthite–water. *Geochim. Cosmochim. Acta* **43**, 1131–1140.

Mojzsis S. J., Harrison T. M. and Pidgeon R. T. (2001) Oxygen-isotope evidence from ancient zircons for liquid water at the Earth's surface 4300 Myr ago. *Nature* **409**, 178–181.

Onasch C. M. and Vennemann T. W. (1995) Disequilibrium partitioning of oxygen isotopes associated with sector zoning in quartz. *Geology* **23**, 1103–1106.

Palin J. M., Epstein S. and Stolper E. M. (1996) Oxygen isotope partitioning between rhyolitic glass/melt and CO2: An experimental study at 550–950 °C and 1 bar. *Geochim. Cosmochim. Acta* **60**, 1963–1973.

Schütze (1980) Der Isotopenindix-eine Inkrementenmethode zur naherungsweise Berechnumg von Isotopenaustauschgleichgewichten zwischen kristallinen Substanzen. *Chemie der Erde* **39**, 321–334.

Shahar A., Young E. D. and Manning C. E. (2008) Equilibrium high-temperature Fe isotope fractionation between fayalite and magnetite: an experimental calibration. *Earth Planet. Sci. Lett.* **268**, 220–338.

Sharp Z. D. and Kirschner D. L. (1994) Quartz-calcite oxygen isotope thermometry: a calibration based on natural isotopic variations. *Geochim. Cosmochim. Acta* **58**, 4491–4501.

Smyth J. R. (1989) Electrostatic characterization of oxygen sites in minerals. *Geochim. Cosmochim. Acta* **53**, 1101–1110.

Spicuzza M. J., Valley J. W., Kohn M. J., Girard J. P. and Fouillac A. M. (1998) The rapid heating, defocused beam technique: a CO_2-laser-based method for highly precise and accurate determination of $\delta^{18}O$ values of quartz. *Chem. Geol.* **144**, 195–203.

Stolper E. and Epstein S. (1991) An experimental study of oxygen isotope partitioning between silica glass and CO_2 vapor. In *Stable isotope geochemistry: A tribute to Samuel Epstein* (ed. H.P. Taylor et al.) *Geochem Soc Spec Publ. No*. **3**, 35–51.

Sessions A. L., Brady J. B. and Chamberlain C. P. (1996) Experimental calibration of an oxygen isotope fractionation factor for zircon. *Geol. Soc. Am Abstr.* **28**, 213.

Taylor H. P. and Epstein S. (1962a) Relationships between $^{18}O/^{16}O$ ratios in coexisting minerals of magmatic and metamorphic rocks: Part I. Principles and experimental results. *Geol. Soc. Am. Bull.* **73**, 461–480.

Taylor H. P. and Epstein S. (1962b) Relationships between $^{18}O/^{16}O$ ratios in coexisting minerals of magmatic and metamorphic rocks: Part II. Applications to Petrologic problems. *Geol. Soc. Am. Bull.* **73**, 675–694.

Taylor H. P. (1968) The oxygen isotope geochemistry of igneous rocks. *Contrib. Mineral. Petrol.* **19**, 1–71.

Taylor H.P. and Sheppard S.M.F. (1986) Igneous Rocks: I. Processes of isotopic fractionation and isotope systematics, *In* Valley, J. W., H. P. Taylor, and J. R. O'Neil (eds.), Stable isotopes in high pressure geological processes, *Rev. Min*., **16**, 227–271.

Trail D., Mojzsis S.J., Harrison T.M., Schmitt A.K., Watson E.B. and Young E.D. (2007) Constraints on Hadean zircon protoliths from oxygen isotopes, Ti-thermometry, and rare earth elements. *Geochem. Geophys. Geosys*. **8**, Q06014. doi:10.1029/2006GC001449.

Valley J. W., Chiarenzelli J. R. and McLelland J. M. (1994) Oxygen isotope geochemistry of zircon. *Earth Planet Sci. Lett.* **126**, 187–206.

Valley J. W., Kitchen N., Kohn M. J., Niendorf C. R. and Spicuzza M. J. (1995) UWG-2, a garnet standard for oxygen isotope ratios: strategies for high precision and accuracy with laser heating. *Geochim. Cosmochim. Acta* **59**, 5223–5231.

Valley J. W., Bindeman I. N. and Peck W. H. (2003) Empirical calibration of oxygen isotope fractionation in zircon. *Geochim. Cosmochim. Acta* **67**, 3257–3266.

Valley J. W., Lackey J. S., Cavosie A. J., Clechenko C. C., Spicuzza M. J., Basei M. A. S., Bindeman I. N., Ferreira V. P., Sial A. N., King E. M., Peck W. H., Sinha A. K. and Wei C. S. (2005) 4.4 billion years of crustal maturation: oxygen isotope ratios of magmatic zircon. *Contrib. Min. Petrol.* **150**, 561–580.

Watson E. B. (1996) Dissolution, growth and survival of zircons during crustal fusion: kinetic principles, geological models and implications for isotopic inheritance. *Trans. R. Soc. Edinburgh: Earth Sci.* **87**, 43–56.

Watson E. B. and Harrison T. M. (1983) Zircon saturation revisited: temperature and composition effects in a variety of crustal magma types. *Earth Planet. Sci. Lett.* **64**, 295–304.

Watson E. B. and Liang Y. (1995) A simple model for sector zoning in slowly-grown crystals: Implications for growth rate and lattice diffusion, with emphasis on accessory minerals in crustal rocks. *Am. Mineral.* **80**, 1170–1187.

Watson E. B. and Cherniak D. J. (1997) Oxygen diffusion in zircon. *Earth Planet. Sci. Lett.* **148**, 527–544.

Watson E. B. (2004) A conceptual model for near-surface kinetic controls on the trace-element and stable isotope composition of abiogenic calcite crystals. *Geochim. Cosmochim. Acta* **68**, 1473–1488.

Watson E. B. and Harrison T. M. (2005) New thermometer reveals minimum melting conditions on earliest Earth. *Science* **308**, 841–844.

Watson E. B., Wark D. A. and Thomas J. B. (2006) Crystallization thermometers for zircon and rutile. *Contrib. Mineral. Petrol.* **151**, 413–433.

Wiedenbeck M., Hanchar J. M., Peck W. H., Sylvester P., Valley J. W., Whitehouse M., Kronz A., Morishita Y., Nasdala L., Fiebig J., Franchi I., Girard J. P., Greenwood R. C., Hinton R., Kita N., Mason P. R. D., Norman M., Ogasawara M., Piccoli R., Rhede D., Satoh H., Schulz-Dobrick B., Skar O., Spicuzza M. J., Terada K., Tindle A., Togashi S., Vennemann T., Xie Q. and Zheng Y. F. (2004) Further characterisation of the 91500 zircon crystal. *Geostand. Geoanal. Res.* **28**, 9–39.

Wilde S. A., Valley J. W., Peck W. H. and Graham C. M. (2001) Evidence form detrital zircons for the existence of continental crust and oceans 4.4 Ga ago. *Nature* **409**, 175–178.

Zhao Z. F. and Zheng Y. F. (2003) Calculation of oxygen isotope fractionation in magmatic rocks. *Chem. Geol.* **193**, 59–80.

Zheng Y. F. (1991) Calculation of oxygen isotope fractionation in metal-oxides. *Geochim. Cosmochim. Acta* **55**, 2299–2307.

Zheng Y. F. (1993) Calculations of oxygen isotope fractionation in anhydrous silicate minerals. *Geochim. Cosmochim. Acta* **57**, 1079–1091.

Associate editor: Thomas Chacko